

RESEARCH

Open Access



Synphilin-1 regulates mechanotransduction in rigidity sensing through interaction with zyxin

Seok Gi Kim^{1†}, Jinyan Li^{2†}, Ji Su Hwang^{1†}, Muhammad Anwar Ul Hassan², Ye Eun Sim³, Ju Yeon Lee⁴, Jung-Soon Mo^{3,5}, Myeong Ok Kim⁶, Gwang Lee^{1,7*} and Sungsu Park^{2,8,9*}

Abstract

Background Synphilin-1 has been studied extensively in the context of Parkinson's disease pathology. However, the biophysical functions of synphilin-1 remain unexplored. To investigate its novel functionalities herein, cellular traction force and rigidity sensing ability are analyzed based on synphilin-1 overexpression using elastomeric pillar arrays and substrates of varying stiffness. Molecular changes are analyzed using RNA sequencing-based transcriptomic and liquid chromatography-tandem mass spectrometry-based proteomic analyses.

Results Synphilin-1 overexpression reduces cell area, with a decline of local contraction on elastomeric pillar arrays. Cells overexpressing synphilin-1 exhibit an impaired ability to respond to substrate rigidity; however, synphilin-1 knockdown restores rigidity sensing abilities. Integrated omics analysis and in silico prediction corroborate the phenotypic alterations induced by synphilin-1 overexpression at a biophysical level. Zyxin emerges as a novel synphilin-1 binding protein, and synphilin-1 overexpression reduces the nuclear translocation of yes-associated protein.

Conclusion These findings provide novel insights into the biophysical functions of synphilin-1, suggesting a potential protective role to the altered extracellular matrix, which may be relevant to neurodegenerative conditions such as Parkinson's disease.

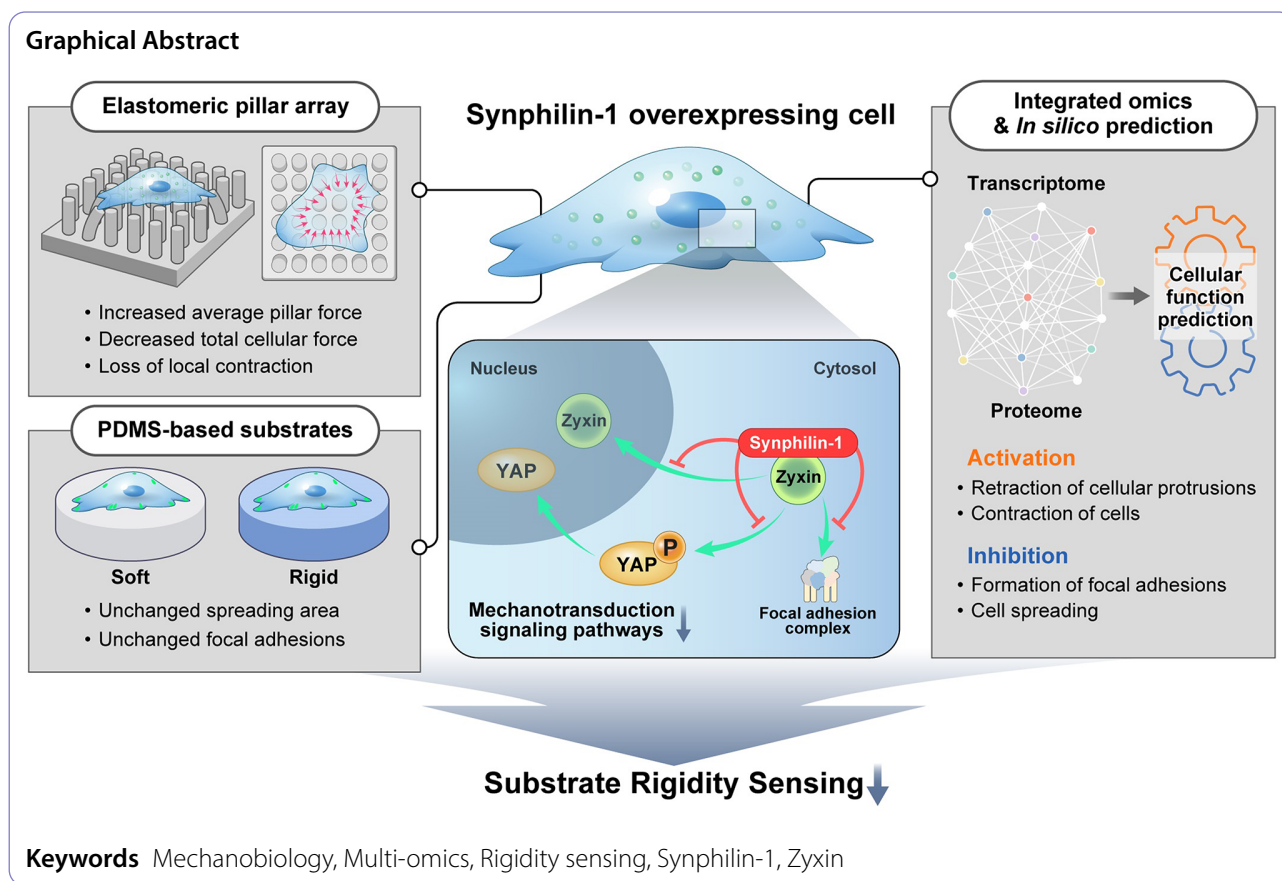
[†]Seok Gi Kim, Jinyan Li and Ji Su Hwang contributed equally to this work.

*Correspondence:
Gwang Lee
glee@ajou.ac.kr
Sungsu Park
nanopark@skku.edu

Full list of author information is available at the end of the article



© The Author(s) 2025. **Open Access** This article is licensed under a Creative Commons Attribution-NonCommercial-NoDerivatives 4.0 International License, which permits any non-commercial use, sharing, distribution and reproduction in any medium or format, as long as you give appropriate credit to the original author(s) and the source, provide a link to the Creative Commons licence, and indicate if you modified the licensed material. You do not have permission under this licence to share adapted material derived from this article or parts of it. The images or other third party material in this article are included in the article's Creative Commons licence, unless indicated otherwise in a credit line to the material. If material is not included in the article's Creative Commons licence and your intended use is not permitted by statutory regulation or exceeds the permitted use, you will need to obtain permission directly from the copyright holder. To view a copy of this licence, visit <http://creativecommons.org/licenses/by-nc-nd/4.0/>.



Introduction

Synphilin-1, identified as an interacting protein of α -synuclein, has been primarily studied in neurons, particularly in the pathology of Parkinson's disease (PD), owing to its presence in Lewy bodies [1–5]. The multifaceted structure of synphilin-1 encompasses several functional domains, including ankyrin-like repeats, a coiled-coil domain, and ATP/GTP-binding motifs [1, 6]. Synphilin-1 interacts with various cytosolic and peripheral membrane proteins, such as PRKN, SIAH, PINK1, AMPK, and SH2D3C [7–13], as well as phospholipids [14]. In addition, synphilin-1 overexpression has been reported to increase neurite outgrowth in mouse neuronal cells [15]. Although synphilin-1 may play a role in membrane and morphological alterations, its biophysical functions require further investigation.

The brain is one of the softest organs in the human body. The softness of the brain is attributed to rich extracellular matrix (ECM) proteins, such as glycoproteins and proteoglycans, which contribute to its low stiffness [16]. However, the composition of ECM can alter under neuropathological conditions [17], affecting tissue mechanics and cellular responses. Notably, changes in ECM protein composition have been observed in the brain tissue of patients with PD [18, 19], yet how these ECM alterations

influence the behavior of brain-resident cells and relate to disease progression remains largely unexplored.

Several platforms and systems have been instituted to evaluate the biophysical and mechanobiological alterations that occur at the single-cell level [20–23]. A particularly efficacious method in this regard involves the assessment of biophysical effects through elastomeric pillar arrays [23, 24]. This approach proves instrumental in the analysis of biophysical functions, given that the nanometric level of pillar deflection facilitates the exploration of the biological responses of cells to mechanical traction forces, rigidity sensing, and physical changes [25–27]. By analyzing cellular forces and their patterns, a comprehensive understanding can be attained regarding the effect of specific factors on the forces and mechanical sensing induced by cells.

Cells within living organisms continuously encounter various types of mechanical stimuli from either their environment or intercellular interactions [28]. In response to these mechanical cues, such as the rigidity of the surrounding substrate, cells regulate diverse functions, including cell morphology, proliferation, and migration, through mechanotransduction pathways [29, 30]. Focal adhesions are integrin-based protein complexes that form the pivotal contact points between cells

and ECM, establishing a connection with actomyosin contractile networks to transmit cellular forces to the matrix [30, 31]. The maturation of focal adhesions from nascent adhesions within protrusive structures, such as lamellipodia and filopodia, induces the formation and extension of lamellipodia structures [28, 32, 33]. Among the components of the focal adhesion complex, zyxin is a representative LIM domain protein with mechanosensitive functions. In response to mechanical stimulation, zyxin regulates actin dynamics, cellular movement, and signal transduction [34–38].

Omics analyses provide comprehensive insights into biological functions [39, 40]. Moreover, integrated omics can compensate the inherent limitations of each single omics. For instance, previous investigations have leveraged integrated omics analyses encompassing transcriptome and metabolome data to propose synphilin-1 functions in the formation of cytoplasmic inclusion bodies, as well as the effect of nanoparticles on cellular traction forces [21, 41].

This study was undertaken to assess the biophysical effects of synphilin-1 in the context of traction force and rigidity sensing using pillar arrays and substrates of different stiffness, as well as to elucidate its biological mechanism using integrated transcriptomic and proteomic analyses. This study was also conducted to analyze the binding between zyxin and synphilin-1 to further investigate the biophysical functionalities of synphilin-1.

Materials and methods

Cell culture and transfection

Human embryonic kidney 293 (HEK293) cells and HEK293 cells stably overexpressing FLAG-synphilin-1 (Synph-293 cells) were cultured in Dulbecco's modified essential medium, supplemented with 10% fetal bovine serum (Corning, NY, USA), penicillin (100 units/mL), and streptomycin (100 µg/mL) (Thermo Fisher Scientific, Waltham, MA, USA) [42]. Cells were cultured at 37 °C and 5% CO₂ in a humidified incubator. HEK293 cells were transfected with empty and FLAG-synphilin-1 vectors using Lipofectamine 3000 (Invitrogen, Waltham, MA, USA), according to the manufacturer's instructions. Scrambled siRNA control and synphilin-1 siRNA were obtained from Dharmacon (Lafayette, CO, USA). Subsequently, HEK293 and Synph-293 cells were transfected with the siRNAs using Lipofectamine RNAiMAX (Invitrogen), according to the manufacturer's instructions.

Scanning electron microscopy (SEM)

HEK293 and Synph-293 cells were fixed with SEM Fixative (1% paraformaldehyde and 2% glutaraldehyde in sodium cacodylate buffer (0.1 M)) for 2 h at 20 °C. Following fixations, cells were rinsed thrice with SEM Fixative and subjected to post-fixation with 1% osmium tetroxide

(Polysciences, Warrington, PA, USA) in sodium cacodylate buffer (0.1 M) for 1 h at 20 °C. Subsequently, each sample was dehydrated in a series of ethanol solutions (50–100%). Next, samples were dried via treatment with hexamethyldisilazane solution (Sigma-Aldrich, St. Louis, MO, USA) twice for 3 min at 20 °C. Finally, samples were coated with gold particles using a coater (Q150R ES; Quorum Technologies, UK). SEM images were acquired using a field emission SEM (Sigma 500; Carl Zeiss, Oberkochen, Germany) at the Three-Dimensional Immune System Imaging Core Facility at Ajou University.

Immunocytochemistry

Coverslips were coated with a solution containing fibronectin (0.01 mg/mL), collagen I (0.03 mg/mL), and bovine serum albumin (0.01 mg/mL) for 1 h at 20 °C on an orbital shaker (M71735; Barnstead Thermolyne Corporation, Dubuque, IA, USA). Cells were seeded onto coverslips and incubated for 12 h at 37 °C with 5% CO₂. Subsequently, cells were fixed and permeabilized using fixation/permeabilization solution (BD bioscience, San Jose, CA, USA) for 30 min at 4 °C. Non-specific background was blocked with phosphate-buffered saline (PBS) containing 2% BSA and 0.1% Triton-X100 for 2 h at RT. Primary antibodies, including anti-synphilin-1 (sc-365741; Santa Cruz Biotechnology, Santa Cruz, CA, USA), anti-FLAG M2 (F1804; Sigma-Aldrich), anti-paxillin (NBP2-57097; Novus Biologicals, Littleton, CO, USA), anti-zyxin (GTX132295; GeneTex, Irvine, CA, USA), and anti-YAP1 (GTX129151; GeneTex) were used at a dilution of 1:400 in blocking buffer. Secondary antibodies, including Alexa Fluor 488 conjugated anti-Rabbit IgG (A-11034; Invitrogen) and Alexa Fluor 546 conjugated anti-Mouse IgG (A-11030; Invitrogen), were used at a dilution of 1:400 in blocking buffer. For F-actin staining, Alexa Fluor 488 phalloidin (A-12379; Invitrogen) and Alexa Fluor 594 phalloidin (A-12381; Invitrogen) were used at a dilution of 1:400 in blocking buffer. Hoechst 33,342 (Invitrogen) at a concentration of 2 µg/mL in PBS was used for nucleus staining. Samples were mounted on ProLong Gold Antifade Mountant (Invitrogen), and images were acquired using a confocal laser-scanning microscope (LSM900; Carl Zeiss) at the Three-Dimensional Immune System Imaging Core Facility at Ajou University. Further image processing and analysis were performed using ZEN 3.2 blue edition software (Carl Zeiss) and the Fiji/ImageJ software [43]. The scatterplot and Pearson correlation coefficient value were obtained using the Colocalization Finder plugin in Fiji/ImageJ software.

Polydimethylsiloxane (PDMS) substrate Preparation

PDMS substrates were prepared using the Sylgard Silicone Elastomer Kit (Dow Corning, Midland, MI, USA)

described previously [29]. The silicone elastomer base was mixed with a curing agent (Sylgard 184; Dow Corning) and degassed for 30 min. The resulting mixture was spin-coated onto a glass bottom confocal dish at 2,000 rpm for 2 min, resulting in a PDMS layer with a thickness of $35 \pm 5 \mu\text{m}$. Subsequently, the elastomer was cross-linked at 70°C for 4 h. Next, the ratio of the elastomer base to the curing agent was adjusted to achieve substrates with distinct Young's moduli. For the "rigid" substrate (2 MPa), the ratio was set to 10:1, whereas for the "soft" substrate (5 kPa), it was adjusted to 75:1. Next, the prepared substrates were functionalized with $20 \mu\text{g}/\text{mL}$ of fibronectin (Sigma-Aldrich) overnight at 4°C . Prior to cell seeding, the PDMS-coated coverslips were washed with PBS and cell culture medium.

Elastomeric pillar array fabrication

Photolithography was used to fabricate a silicon wafer mold featuring an array of holes (diameter: 500 nm, depth: $1.3 \mu\text{m}$, and center-to-center distance: $1 \mu\text{m}$) for pillar array fabrication, as described previously [21, 44]. The fabrication process involved mixing PDMS with a curing agent in a 10:1 ratio to achieve Young's modulus of 2 MPa. This mixture was vacuumed for 15 min to remove bubbles. Subsequently, the mixture was spin-coated onto the mold at 500 rpm for 10 s and at 1,800 rpm for 30 s, followed by an additional 30 min vacuum cycle to eliminate any remaining bubbles. Next, the PDMS-coated mold was cured at 80°C for 3 h. Each resulting pillar possessed a bending stiffness (k) of $8.4 \text{ nN}/\mu\text{m}$. The bending stiffness of the pillars was calculated based on the Euler-Bernoulli beam theory (Eq. (1)) [45]:

$$k = \frac{3}{64} \pi E \frac{D^4}{L^3} \quad (1)$$

where E represents Young's modulus, D indicates the pillar diameter, and L denotes the pillar length.

Subsequently, pillars were functionalized with fibronectin ($20 \mu\text{g}/\text{mL}$) (Sigma-Aldrich) overnight at 4°C . Prior to cell seeding, the pillar array was washed with PBS and cell culture medium.

Pillar displacement measurement

Cells on the pillar arrays were cultured in a live-cell chamber (Live Cell Instrument, Seoul, Korea) at 37°C with 5% CO_2 . Imaging was conducted using an inverted microscope (ECLIPSE TE2000-U, Nikon) equipped with a high-speed camera (BFS-U3-32S4M-C; FLIR, Wilsonville, OR, USA) to capture pillar movements at 100 frames/s. A 10 s movie consisting of 1,000 frames was recorded for each cell. Pillar displacements were analyzed using the PillarTracker plugin from the Mechanobiology Institute in Singapore, enabling the calculation of

traction force for individual pillars. The traction force (F) was calculated using the following formula (Eq. (2)):

$$F = k \times \Delta x \quad (2)$$

Local contraction was quantified by assessing the directional parameter (γ) of adjacent two pillar pairs during the initial 30-min cell spreading phase at the leading edge [27]. The directional parameter (γ) was calculated as the sum of the pillar force vectors divided by the sum of their magnitudes. When considering two neighboring pillar forces, A and B (Fig. 2B), the formula for γ is expressed as follows (Eq. (3)):

$$\gamma = \frac{\sqrt{(Ax + Bx)^2 + (Ay + By)^2}}{\sqrt{Ax^2 + Ay^2} + \sqrt{Bx^2 + By^2}} \quad (3)$$

A group of eight pillars was defined as the region for analysis, with four such regions analyzed per cell.

RNA sequencing

For RNA sequencing library preparation, $1 \mu\text{g}$ of total RNA from cells was used employing the TruSeq Stranded mRNA Sample Prep Kit (Illumina, San Diego, CA, USA). RNA molecules were fragmented and synthesized as single-stranded cDNAs through random hexamer priming, followed by the preparation of double-stranded cDNA. Following the sequential process of end repair, A-tailing, and adapter ligation, cDNA libraries were amplified with PCR. The quality of the cDNA libraries was evaluated using Agilent 2100 BioAnalyzer (Agilent Technologies, Palo Alto, CA, USA). cDNA library quantification was performed using a KAPA library quantification kit (Kapa Biosystems, Wilmington, MA, USA). After cluster amplification, the sequencing progressed as paired-end ($2 \times 150 \text{ bp}$) using the Illumina Novaseq6000 platform (Illumina).

RNA extraction and RT-qPCR

Total RNA was isolated from HEK293 and Synph-293 cells using the Direct-Zol RNA Miniprep kit (Zymo Research, Irvine, CA, USA). Isolated RNA was converted to a cDNA library using the iScript Advanced cDNA Synthesis Kit (Bio-Rad, Hercules, CA, USA) and a thermocycler (T3000; Biometra, Jena, Germany). Gene expression levels associated with the transcriptomic network were acquired via quantitative reverse transcription PCR using SsoAdvanced™ Universal SYBR® Green Supermix real-time PCR Kit (Bio-Rad) and Rotor Gene-Q 5plex HRM (Qiagen, Valencia, CA, USA). Relative quantification of gene expression levels was calculated using the $2^{-\Delta\Delta\text{Ct}}$ method. Primer sequences are provided in Supplementary Table 1.

Liquid chromatography-tandem mass spectrometry

HEK293 and Synph-293 cells were lysed in RIPA buffer (Thermo Fisher Scientific). Subsequently, RIPA buffer was removed from cell lysates via centrifugation. The samples were denatured and reduced with urea (8 M) and tris(2-carboxyethyl)phosphine hydrochloride (8 mM) for 1 h at 20 °C. Next, the samples were alkylated using iodoacetamide (15 mM) for 1 h at 20 °C in the dark. Following alkylation, trypsin digestion was conducted for 16 h at 37 °C. Each sample was labeled with a tandem mass tag (TMT)-6-plex (126, 127, 128, 129, 130, 131) according to the manufacturer's protocol, and the combined TMT-labeled sample was fractionated by high-pH reversed-phase liquid chromatography (Nexera XR; Shimadzu, Kyoto, Japan) with a C₁₈ column (Shimadzu). All fractions were collected using an FRC-10 A fraction collector (Shimadzu) and desalted using Macro SpinColumns (Harvard Apparatus, Holliston, MA, USA). TMT-labeled peptides were quantified using an Orbitrap Fusion Lumos mass spectrometer (Thermo Fisher Scientific) and a nano-electrospray source (Thermo Fisher Scientific) equipped with Easy nLC 1200 (Thermo Fisher Scientific). Peptides were trapped using a C₁₈ pre-column (Thermo Fisher Scientific) and separated using a C₁₈ reverse-phase column (Thermo Fisher Scientific) at a flow rate of 300 nL/min with mobile phase A and B of 0% and 80% acetonitrile containing 0.1% formic acid respectively. During chromatographic separation, Orbitrap Fusion Lumos mass spectrometer acquired MS and MS/MS data in the data-dependent mode, repeatedly switching 3 s cycle time.

Identification and quantification for proteome data

ProLucid [46] was used to identify the peptide protocols with the UniProt human protein database (January 2018, Reviewed proteins) from MS/MS spectra data. A precursor mass error of 5 ppm, and a fragment ion mass error of 200 ppm. Trypsin was selected as the enzyme, with two potential missed cleavages. TMT modification (+229.1629) at the N-terminus and lysine residue by the labeling reagent and carbamidomethylation at cysteine were chosen as static modifications. Oxidation at methionine was chosen as variable modification. Reporter ions were extracted from small windows (± 20 ppm) around their expected *m/z* in the HCD spectrum. The reversed sequences of all proteins were appended into the database for calculation of the false discovery rate. The output data files were filtered and sorted to compose the protein list using the DTASelect [47] (The Scripps Research Institute, USA) with two or more peptide assignments for protein identification and a false positive rate of less than 0.01.

For quantitative analysis, a Census within the IP2 pipeline (Integrated Proteomics, USA) was used. The

intensity at a reporter ion channel for each protein was calculated as the sum of this reporter ion's intensities from all constituent peptides from the identified protein [48]. TMT ratios for proteins were determined by summing reporter ion intensities across all peptides assigned to a protein subgroup. Reversed and potential contaminant proteins were excluded from the analysis.

Formaldehyde cross-linking and co-immunoprecipitation

HEK293 and Synph-293 cells were subjected to protein cross-linking via incubation with 1% formaldehyde solution at 20 °C for 10 min on an orbital shaker. After washing with PBS, the cross-linking reaction was quenched using Tris/PBS buffer (0.5 M) at RT for 5 min on a shaker. The cells were washed with PBS and lysed with RIPA buffer (Thermo Fisher Scientific), supplemented with Protease Inhibitor Cocktail Solution (GenDEPOT, Katy, TX, USA) and Phosphatase Inhibitor Cocktail Solution (GenDEPOT) for 1 h at 4 °C. Subsequent processes were conducted using protein G-Sepharose beads (Millipore, Billerica, MA, USA). Cell lysates were centrifuged, and the supernatants were collected. Protein concentrations of samples were measured using the BCA Protein Assay Kit (Thermo Fisher Scientific) to ensure an equal amount of protein in each sample. Each sample was incubated with an anti-zyxin antibody (sc-293448; Santa Cruz Biotechnology) or anti-synphilin-1 antibody (sc-365741; Santa Cruz Biotechnology) overnight at 4 °C. Post-incubation with antibodies, samples were incubated with protein G-Sepharose beads for 1 h at 4 °C. The beads were washed thrice, and conjugated proteins were eluted using Lane Marker Reducing Sample Buffer (39000; Thermo Fisher Scientific). The following antibodies were used for western blotting analysis: anti-synphilin-1 (1:500) (sc-365741; Santa Cruz Biotechnology), anti-FLAG M2 (1:500) (F1804; Sigma-Aldrich), and anti-zyxin (1:1000) (GTX132295; GeneTex).

Single protein and protein-protein structure prediction

The AlphaFold Server (AlphaFold 3) was used to predict single protein as well as protein-protein structures [49]. The following human protein sequences were obtained from the UniProt database [50]: synphilin-1 (Q9Y6H5), zyxin (Q15942), and paxillin (P49023). The results of single protein and protein-protein structure prediction were visualized using the PyMOL software (The PyMOL Molecular Graphics System, Version 2.5.4 Schrödinger, LLC).

Statistical analysis

Statistical significance was determined using the IBM SPSS Statistics 20 software (IBM Corporation, Armonk, NY, USA). An independent sample *t*-test with Levene's test was performed to analyze the differences between

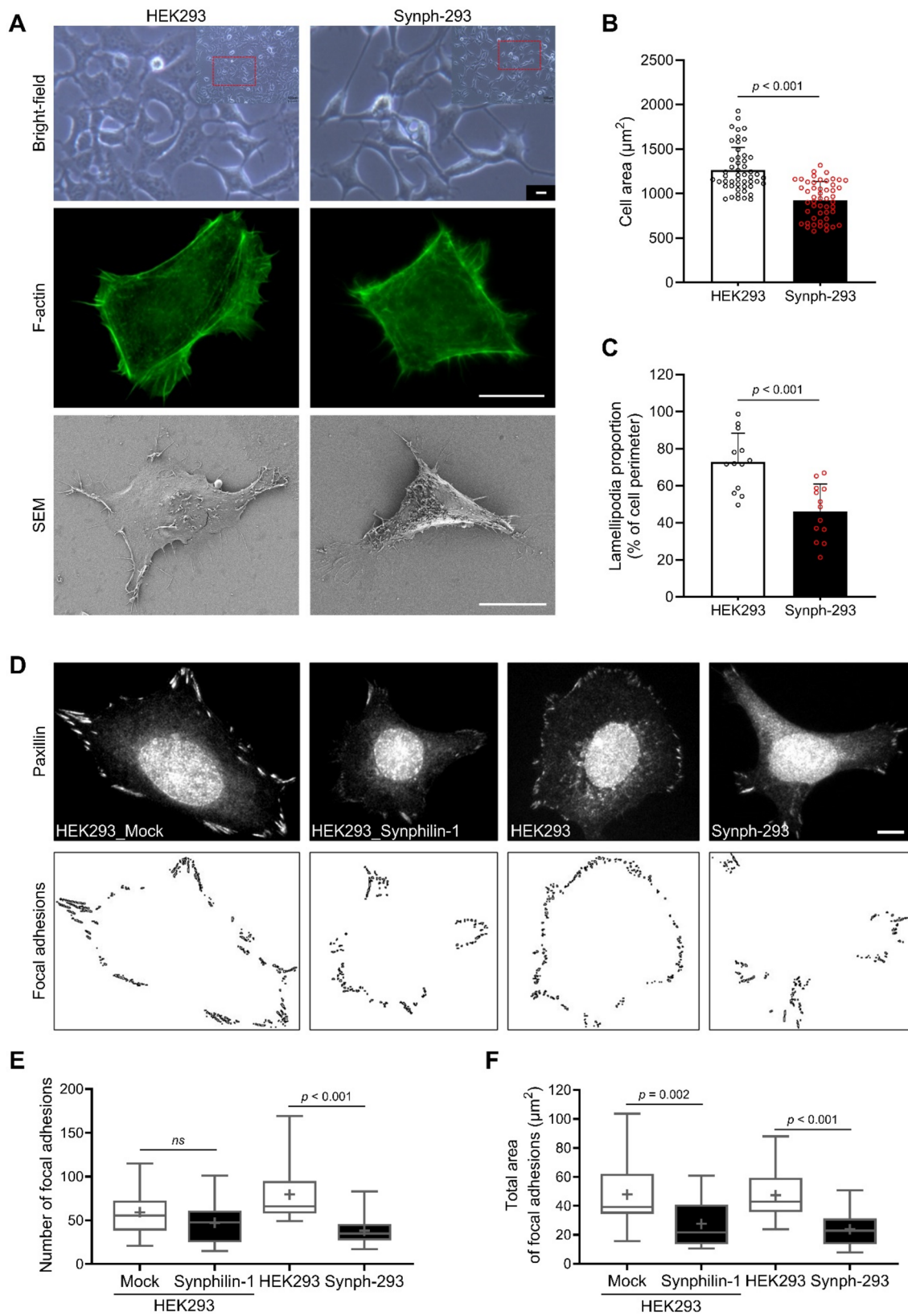


Fig. 1 (See legend on next page.)

(See figure on previous page.)

Fig. 1 Cells overexpressing synphilin-1 exhibited reduced spreading area with decreased lamellipodia formation and focal adhesion. **A** Cell morphology of human embryonic kidney 293 (HEK293) and synphilin-1-overexpressing HEK293 (Synph-293) cells from bright-field, F-actin staining, and scanning electron microscopy analyses (scale bars: 20 μm). **B** Cell spreading area of HEK293 and Synph-293 cells ($n=50$). Data represent the mean + SD. **C** Proportion of lamellipodia structures at the edge of HEK293 and Synph-293 cells ($n=13$). Data represent the mean + SD. Individual value is represented as a hollow circle. **D** Focal adhesion analysis of cells using paxillin staining images (scale bar: 10 μm). **E, F** Number (**E**) and total area (**F**) of focal adhesions of cells ($n=24/18/31/47$). The inner solid line and cross sign indicate the median and mean values, respectively. Statistical significance was determined using an independent sample *t*-test with Levene's test. *ns*: no significance

two experimental groups. Statistical differences among multiple (≥ 3) experimental groups were determined using a one-way analysis of variance (ANOVA), followed by Tukey's HSD or Games-Howell *post-hoc* pairwise comparisons.

Results

Synphilin-1 overexpressing cells exhibited reduced spreading area with decreased lamellipodia formation and focal adhesion

HEK293 and FLAG-tagged synphilin-1 (FLAG-synphilin-1) overexpressing HEK293 (Synph-293) cell lines were used for the overall analyses regarding the assessment of the biophysical functions of synphilin-1 (Supplementary Fig. 1A) [42]. The most prominent change observed in Synph-293 cells was a decrease in cell spreading area accompanied by morphological changes (Fig. 1A). F-actin staining and SEM image analysis revealed that Synph-293 cells exhibited a contracted cellular shape with fewer lamellipodia-like protrusions compared to HEK293 cells. The spreading area of Synph-293 cells was significantly smaller than that of HEK293 cells (Fig. 1B). In addition, the spreading area was reduced in HEK293 and SH-SY5Y (human neuroblastoma cell) cells transiently overexpressing the FLAG-synphilin-1 (isoform 1, complete sequence) and GFP-tagged synphilin-1 (isoform 5, containing whole domains) (Supplementary Fig. 1B, C). The SEM images revealed that the proportion of lamellipodia in the total cell perimeter was also notably lower in Synph-293 cells than in HEK293 cells (Fig. 1C; Supplementary Fig. 1D, E).

Subsequently, we analyzed the focal adhesion patterns using paxillin staining and image processing in transiently or stably synphilin-1 overexpressing HEK293 cells (Fig. 1D). Following transfection, transiently FLAG-synphilin-1 overexpressing HEK293 cells exhibited a tendency towards decreased focal adhesion number, with stably FLAG-synphilin-1 overexpressing Synph-293 cells demonstrating a significant reduction compared to HEK293 cells (Fig. 1E). Notably, both transiently and stably FLAG-synphilin-1-overexpressing cells exhibited a significant decrease in the total area of focal adhesions (Fig. 1F). The images of co-staining with F-actin and paxillin showed that stress fiber structures associated with focal adhesion were observed in HEK293 cells, but stress fibers were not well observed in Synph-293 cells, even though focal adhesion was observed (Supplementary

Fig. 1F). Decreased focal adhesion tendency was also observed in FLAG-tagged synphilin-1 transfected SH-SY5Y cells (Supplementary Fig. 1G). These results suggest that synphilin-1 overexpression reduced cell spreading area by attenuating the formation of lamellipodia structures and focal adhesions.

Synphilin-1 overexpression induced cellular contraction towards the central region with diminished local contractions

Subsequent detailed analyses of cellular traction force were conducted by placing cells on elastomeric pillar arrays, with force applied by each cell to the pillars being calculated (Fig. 2A). Additionally, the directionality (γ) of pillars was analyzed based on the direction pattern of adjacent pillars (Fig. 2B) [27]. To assess the reversible effect of synphilin-1 overexpression, synphilin-1-knockdown Synph-293 (Synph-293-KD) cells were co-analyzed with HEK293 and Synph-293 cells (Supplementary Fig. 2A, B). Prior to pillar array analysis, the morphological observation of Synph-293-KD cells showed that synphilin-1 knockdown in Synph-293 cells reversed cell morphology, restoring a phenotype similar to HEK293 cells (Supplementary Fig. 2C). Incubation of cells on the pillar arrays revealed significant phenotypic differences among HEK293, Synph-293, and Synph-293-KD cells (Fig. 2C). Compared to HEK293 cells, Synph-293 cells occupied fewer pillars, indicative of a smaller spreading area (Fig. 2D). Furthermore, at the edge of the cell, pillars beneath Synph-293 cells exhibited considerably greater displacement towards the central axis. The average traction force exerted on pillars beneath Synph-293 cells was significantly higher than that observed in HEK293 cells (Fig. 2E). However, the total traction force exhibited by Synph-293 cells was dramatically decreased compared to HEK293 cells (Fig. 2F). Notably, the Synph-293-KD cells exhibited a tendency to revert to HEK293 cells, encompassing trends of significantly higher pillar occupancy and a lower average traction force than Synph-293 cells (Fig. 2C–E).

Several studies have evaluated cellular substrate rigidity sensing by measuring local contractions on pillar arrays [27, 29, 51]. In the early spreading phase of cells, locally contracted units formed at the leading edges of cells to sense substrate rigidity. Analysis of pillar displacement patterns at the edge of each cell revealed that Synph-293 cells exhibited a diminished frequency of locally

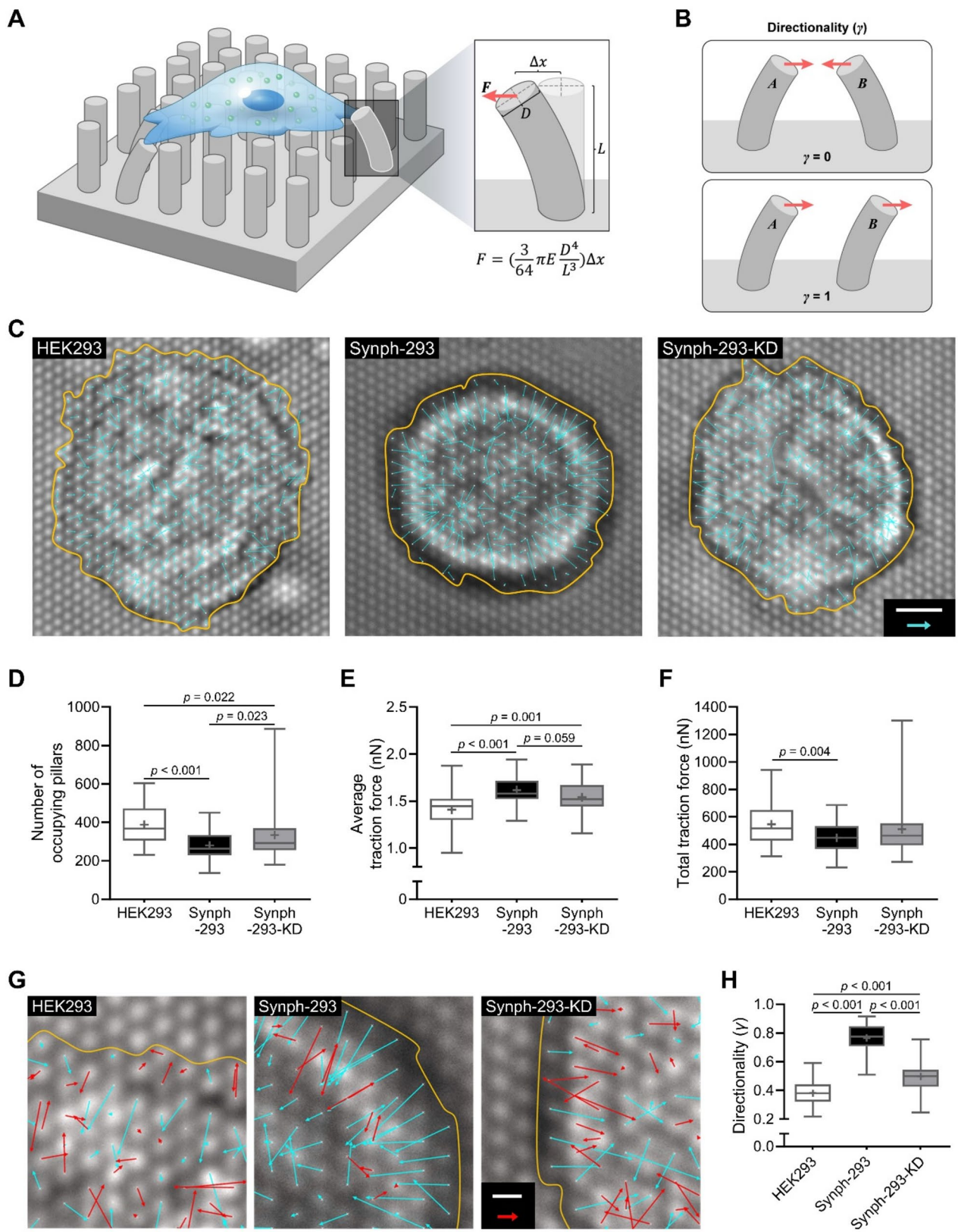


Fig. 2 (See legend on next page.)

(See figure on previous page.)

Fig. 2 Synphilin-1 overexpression induced cellular contraction toward the center, with diminished local contraction. **A** Schematic representation of elastomeric pillar arrays and pillar force formula. **B** Schematic representation of the directionality (γ) of pillars. **C** Pillar deflection map of HEK293, Synph-293, and synphilin-1-knockdown Synph-293 (Synph-293-KD) cells (scale bar: 4 μm) (scale arrow: 3 nN). The yellow line indicates the cell boundary. The length and direction of the cyan arrows indicate the magnitude and direction of traction force vectors, respectively. **D** Number of pillars covered by cells ($n=50$). **E** Average traction force of pillars beneath cells ($n=50$). **F** Total traction force of pillars beneath cells ($n=50$). **G** Spatial traction force distribution at the edge of cells (scale bar: 1 μm) (scale arrow: 1 nN). Red arrows indicate contractile units. **H** γ analysis of the pillars of the edge of cells ($n=50$). The inner solid line and cross sign indicate the median and mean values, respectively. Statistical significance was determined using a one-way ANOVA, followed by Tukey's HSD comparison test

contracted pillar pairs of similar magnitudes compared to HEK293 cells (Fig. 2G). In contrast, Synph-293-KD cells demonstrated an increase in the frequency of locally contracted pillar pairs. The γ values of pillars were numerically calculated, yielding a directionality parameter (Fig. 2H); the γ value for the edge region of Synph-293 cells was significantly higher and closer to 1 than that of HEK293 cells, whereas γ value for Synph-293-KD cells was reduced compared to that for Synph-293 cells. In addition, high-speed photographs of pillars revealed the step-fitted pillar pair [51], indicative of simultaneous displacement towards each other, in HEK293 and Synph-293-KD cells but not in Synph-293 cells (Supplementary Fig. 2D, E). Our pillar array results suggest that cells overexpressing synphilin-1 may exhibit impaired probing of substrate rigidity owing to the loss of contractile units at the cell edge.

Synphilin-1 overexpression attenuated cellular rigidity sensing across substrates with different stiffness

Considering the potential involvement of synphilin-1 in rigidity sensing for a substrate, we investigated the effects of synphilin-1 overexpression on cellular rigidity sensing in substrates with various stiffness. The analysis encompassed flat PDMS-based substrates of 5 kPa and 2 MPa stiffness [29] and a conventional cell culture dish (~ 1.7 GPa). HEK293 cells exhibited an increased spreading area in response to changes in substrate stiffness, underscoring their proficiency in substrate rigidity sensing (Fig. 3A, B). In contrast, Synph-293 cells demonstrated an absence of a significant spreading area alteration in response to changes in substrate stiffness (Fig. 3A, C). However, this unresponsive phenotype in Synph-293 cells was ameliorated upon synphilin-1 knockdown, resulting in an increased cell spreading area according to the stiffer substrate (Fig. 3A, D). In addition, even with synphilin-1 knockdown, HEK293 cells retained their ability to modulate their spreading area in response to substrate stiffness (Supplementary Fig. 2F).

Similar to the cell spreading area, HEK293 cells exhibited an increased focal adhesion area in direct correlation with the stiffness of substrates (Fig. 3E, F). Conversely, Synph-293 cells did not exhibit a significant change in focal adhesion area; however, this unresponsive trait was mitigated by synphilin-1 knockdown, resulting in the restoration of their ability to respond to substrate stiffness

(Fig. 3G, H). Consistent with the trends observed in the cell spreading area, synphilin-1 knockdown in HEK293 cells maintained their proficiency in sensing substrate stiffness (Supplementary Fig. 2G). These results suggest that synphilin-1 overexpression negatively affects substrate rigidity sensing; however, this effect can be reversibly controlled through changes in synphilin-1 expression levels.

Integrated transcriptomics and proteomics analyses predicted the phenotype of synphilin-1 overexpression

The molecular mechanisms behind phenotypic changes induced by synphilin-1 overexpression were elucidated through *in silico* predictions using Ingenuity Pathway Analysis (IPA), incorporating both transcriptome and proteome datasets derived from HEK293 and Synph-293 cells. The transcriptomic analysis revealed 1,012 down-regulated and 1,678 up-regulated genes screened from a pool of 27,869 identified genes, adhering to specific criteria ($p < 0.05$ and fold-change ± 1.5) (Fig. 4A). Similarly, the proteomic analysis revealed 1,231 down-regulated and 1,224 up-regulated proteins selected from 5,151 identified proteins ($p < 0.05$ and fold-change ± 1.2) (Fig. 4B). Transcriptomic analyses predicted activated synaptic signaling, neuronal differentiation, and cell viability, while pathways and biological functions related to cholesterol metabolism, autophagy, and cell death were predicted to be inhibited in Synph-293 cells (Supplementary Figs. 3 and 4). Proteomic analyses predicted the activation of translation and cell survival processes, inhibiting adhesion, apoptosis, and sensitivity responses. Comparative analysis of the biological functions predicted by transcriptomic and proteomic datasets revealed potential morphological changes in cells subsequent to synphilin-1 overexpression (Fig. 4C). Subsequently, networks of biological functions more directly related to the *in vitro* results were constructed using each omics dataset. The transcriptomic network predicted the inhibition of the "formation of focal adhesions" and "cell spreading" coupled with the activation of "retraction of cellular protrusions" and "contraction of cells" involving 121 related genes (Fig. 4D; Supplementary Fig. 5A, B; Supplementary Table 2). Similarly, the proteomic network analysis predicted consistent trends in these four functions, highlighting the contributions of 132 proteins (Fig. 4E; Supplementary Fig. 5D, E; Supplementary Table 3). The

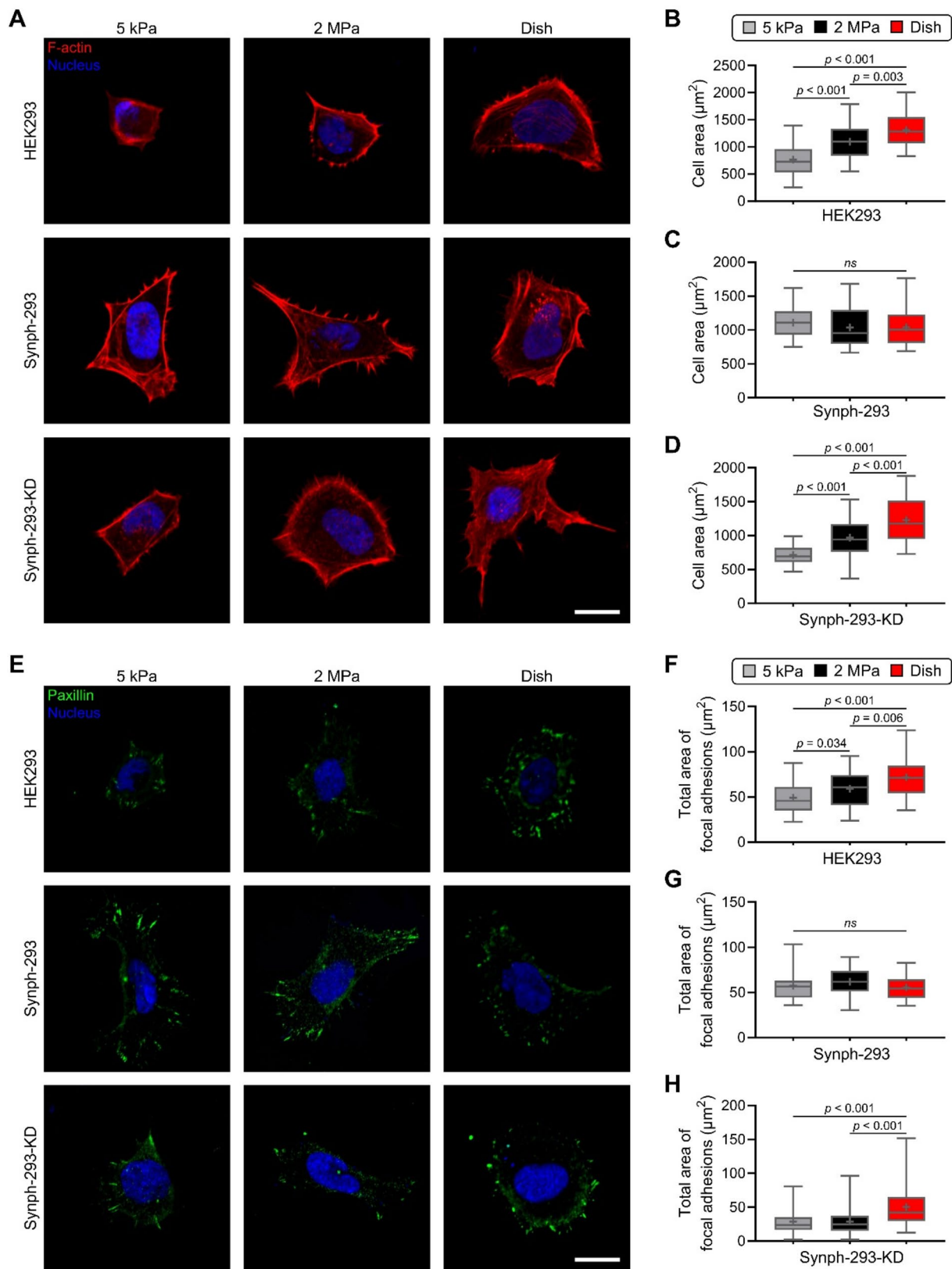


Fig. 3 (See legend on next page.)

(See figure on previous page.)

Fig. 3 Synphilin-1 overexpression induced the loss of cellular rigidity sensing on substrates with different stiffness. **A** Actin staining images of cells on substrates with different stiffness (scale bar: 20 μ m). **B–D** Spreading area of cells on substrates with different stiffness in HEK293 (**B**), Synph-293 (**C**), and Synph-293-KD cells (**D**) ($n=50$). **E** Focal adhesion of cells on substrates with different stiffness (scale bar: 20 μ m). **F–H** Total area of focal adhesions of cells on substrates with different stiffness in HEK293 (**F**), Synph-293 (**G**), and Synph-293-KD cells (**H**) ($n=50$). The inner solid line and cross sign indicate the median and mean values, respectively. Statistical significance was determined using a one-way ANOVA followed by Tukey's HSD (**B, F, G**) and Games-Howell (**C, D, H**) comparison test

expression patterns of the identified genes and proteins within the IPA networks were visually clustered into heat maps (Supplementary Fig. 5C, F). Among the genes included in the transcriptomic network, a quantitative PCR was performed to quantify the expression levels of nine genes deemed to have substantial contributions to the elicited functional changes. Notably, the expression levels of *CCND1*, *F2R*, *INPP5D*, and *RYR2* were significantly higher, and those of *CDKN2A*, *MYO3A*, *PLCB2*, *RHOD*, and *SDC2* were lower in Synph-293 cells than in HEK293 cells, confirming the concordant trends observed in the transcriptomic network (Fig. 4F). Additionally, an assessment of the relative abundance of proteins within the proteomic network revealed increased levels of CD81, GPI, HTT, MAPT, PAK4, and RHOA and decreased levels of AKAP12, ITGB1, LMNA, PXN, SDC2, TPM1, VCL, and YWHAZ in Synph-293 cells (Fig. 4G). An integrated network analysis of the transcriptome and proteome consistently uncovered identical trends across the four cellular functions, providing a comprehensive understanding of the morphological changes observed in Synph-293 cells (Fig. 4H; Supplementary Fig. 6). Overall, omics analysis employing transcriptome and proteome datasets not only strengthened the observed phenotype of synphilin-1 overexpression through in silico prediction but also provided insights into its biological functions at the molecular level.

Synphilin-1 interacted with zyxin in the cytosol and affected the subcellular localization of YAP (yes-associated protein)

Focal adhesion, a complex integral to the formation of cellular protrusions containing lamellipodia, is directly connected to the external environment of the cell [30, 31]. Within the molecular repertoire constituting the focal adhesion complex, LIM domain proteins, such as paxillin and zyxin, play a role in the transduction of mechanical signals [36, 52]. Based on this background, we identified a novel synphilin-1 interacting protein, namely zyxin. Zyxin expression patterns in Synph-293 cells were highly co-localized with synphilin-1 in the cytosolic region (Fig. 5A; Supplementary Fig. 7A, B), with the Pearson correlation coefficient of both fluorescence analyses 0.941 (Fig. 5B) and 0.912 (Supplementary Fig. 7C), respectively. Similar expression patterns were observed in synphilin-1-overexpressing SH-SY5Y cells, yielding a Pearson correlation coefficient of 0.928

(Supplementary Fig. 7D, E). In SH-SY5Y cells expressing GFP (GFP-control) or GFP-synphilin-1, GFP was primarily expressed in the nucleus, whereas GFP-synphilin-1, devoid of nuclear localization, co-localized with zyxin in the cytosol (Supplementary Fig. 7F).

Subsequently, we performed co-immunoprecipitation to validate the physical interaction between synphilin-1 and zyxin. Formaldehyde cross-linking definitively established the presence of binding between zyxin and synphilin-1 (Fig. 5C). This interaction was further substantiated through reciprocal co-immunoprecipitation with zyxin (Fig. 5D). Additionally, FLAG-synphilin-1 co-immunoprecipitation without cross-linking confirmed the direct binding between synphilin-1 and zyxin, whereas paxillin did not show any evidence of binding with synphilin-1 (Supplementary Fig. 8A). Furthermore, the structures of single proteins and protein-protein complexes were predicted from the AlphaFold 3 [49]. The single structure prediction results for zyxin and FLAG-synphilin-1 confirmed that the structure of zyxin comprised three LIM zinc-binding domains, and that of synphilin-1 consisted of one coiled-coil domain and six ankyrin repeats (Fig. 5E, F). Notably, in the structure prediction of zyxin-FLAG-synphilin-1, even the disordered regions of each protein were present close to each other to form a compact structure and appeared to be a single complex (Fig. 5G). A similar pattern was reproduced between zyxin and intact synphilin-1 (Supplementary Fig. 8B, C); however, paxillin-synphilin-1 structure prediction revealed that paxillin and synphilin-1 maintained their respective single protein structures (Supplementary Fig. 8D, E). These results underscore the cytosolic interaction between synphilin-1 and zyxin, suggesting that this interaction may affect the function of zyxin.

Next, we analyzed the relationship between synphilin-1 overexpression and YAP. YAP is renowned as a conserved mechanotransducer capable of sensing external mechanical signals through subcellular relocation [53]. Indeed, zyxin knockdown has been reported to decrease the nuclear localization of YAP [54] and increase Ser127 phosphorylation [54, 55], which is critical for its cytoplasmic sequestration [56, 57]. Immunofluorescence analyses revealed discernible alterations in the subcellular localization patterns of YAP in response to synphilin-1 overexpression (Fig. 5H). Cytosol localization of YAP increased in transiently FLAG-synphilin-1-overexpressing HEK293 cells and in Synph-293 cells on

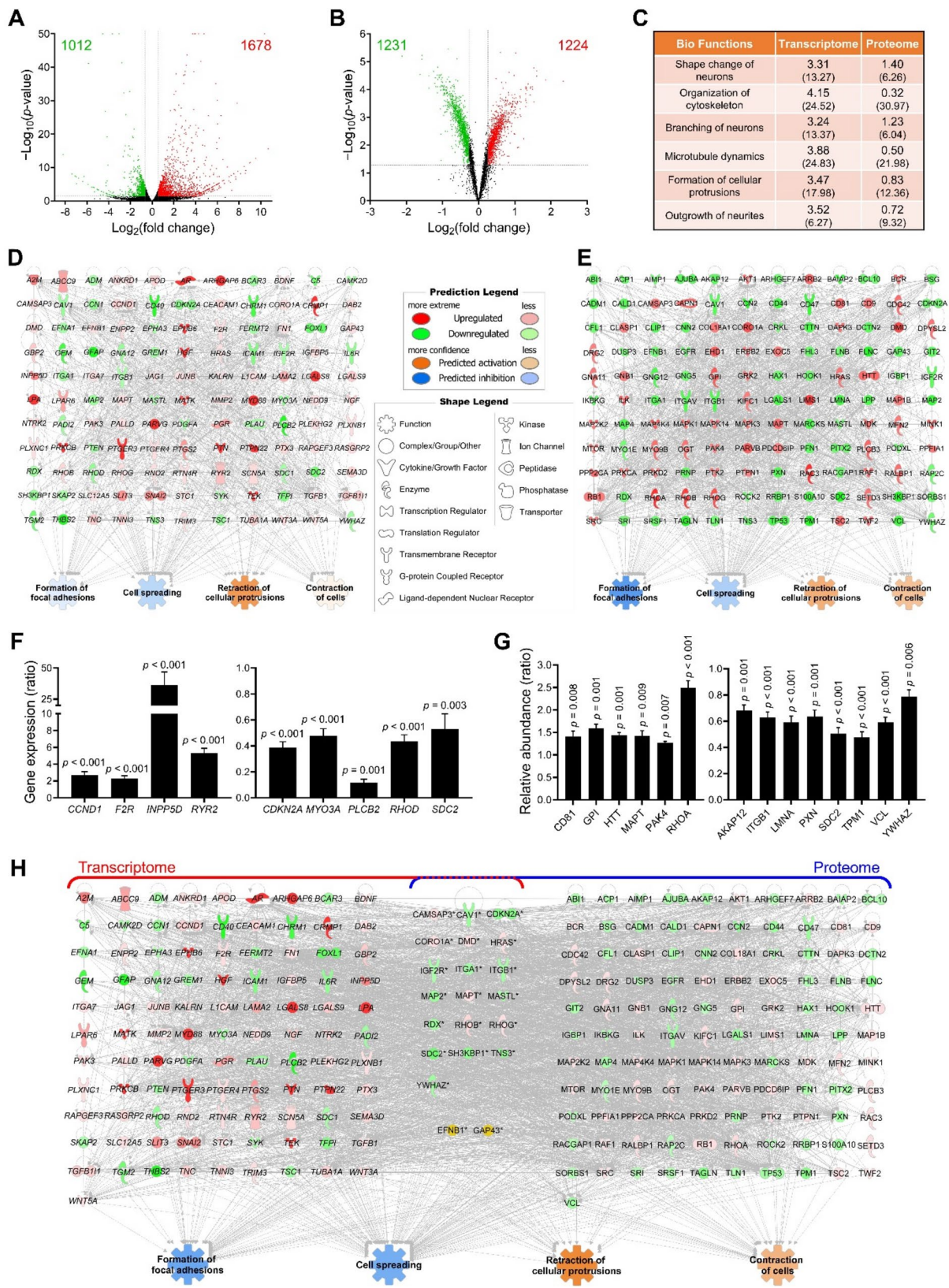


Fig. 4 (See legend on next page.)

(See figure on previous page.)

Fig. 4 Integrated omics analyses encompassing transcriptome and proteome datasets predicted the phenotype of synphilin-1 overexpression. **A** Volcano plot of gene expression. Points satisfying the threshold $p < 0.05$ and fold change ± 1.5 are denoted by green (down-regulated in Synph-293 cells) and red (up-regulated in Synph-293 cells). **B** Volcano plot of protein expression. Points satisfying the threshold $p < 0.05$ and fold change ± 1.2 are denoted by green (down-regulated) and red (up-regulated). **C** Comparison analysis of cellular functions between transcriptome and proteome datasets using Ingenuity Pathway Analysis (IPA) software. Numbers in the table indicate “activation z-score ($-\text{Log}_{10}(p\text{-value})$)”. **D** Transcriptome network with an in silico prediction of Synph-293 cell phenotype using IPA software. **E** Proteome network with Synph-293 phenotype prediction. **F** Gene expression level of transcriptome network-related genes in Synph-293 cells. GAPDH was used as an internal control for gene expression normalization. Data represent the mean \pm SD of three independent experiments. **G** Relative protein abundance levels of proteome network-related proteins in Synph-293 cells. Data represent the mean \pm SD. **H** Integrated omics network with the prediction of cellular functions. Molecules with opposite expression patterns are presented in yellow. Statistical significance was determined using an independent sample *t*-test with Levene’s test

glass substrates, leading to a significant reduction in the expression ratio of nuclear YAP (Fig. 5I). This observed trend was reconfirmed in synphilin-1-overexpressing SH-SY5Y cells with noticeably increased localization of cytosolic YAP (Supplementary Fig. 9A, B). Unlike cells on glass substrates, HEK293 and Synph-293 cells placed on a polyacrylamide (PA) gel with a lower stiffness (~ 50 kPa) exhibited no difference in YAP localization patterns and nuclear expression ratio (Supplementary Fig. 9C, D). On the PA gels, the distribution of YAP expression throughout cells was observed in both cells. Subsequently, the phosphorylation level of YAP (Ser127) of cells on a conventional cell culture dish was analyzed to confirm the molecular change in YAP (Fig. 5J). Transient and stable FLAG-synphilin-1 overexpression resulted in a 1.1- and 1.4-fold increase in phosphorylated YAP (Ser127), respectively (Fig. 5K). Conversely, the total YAP in both conditions exhibited a reduction, showing a 0.9- and 0.8-fold decrease, respectively, compared to each control (Fig. 5L). Furthermore, the phosphorylated YAP level reverted to a decreased state upon synphilin-1 knock-down in Synph-293 cells (Supplementary Fig. 9E). Immunofluorescence and western blotting analyses revealed that synphilin-1 overexpression reduced the nuclear translocation of YAP, constituting the mechanisms underlying mechanotransduction.

Overall, our results suggest that synphilin-1 overexpression impedes substrate rigidity sensing capacity by interacting with zyxin and inhibiting nuclear translocation of YAP (Fig. 6). These findings elucidate the novel biophysical functions of synphilin-1 in regulating substrate rigidity sensing.

Elevated collagen I expression in patients with PD and the protective effects of synphilin-1 overexpression against excessive collagen I

The ECM in the brain plays a crucial role in maintaining tissue structure and function, with alterations in ECM protein composition linked to various neurological diseases. In particular, an increase in collagen I has been observed in the brain tissue of patients with PD [18, 19]. Given that collagen I can significantly increase tissue stiffness [58], we analyzed omics data of collagen I levels from the brain tissue of a patient with PD.

Transcriptomic analyses of the substantia nigra revealed significant upregulation of both collagen type I alpha 1 (COL1A1) and collagen type I alpha 2 (COL1A2) chains in patients with PD [59, 60] (Supplementary Fig. 10A, B). Transcriptomic data from the dorsal striatum, where dopamine neurons project, showed a significant increase in COL1A1 expression in both the putamen and caudate regions [61] (Supplementary Fig. 10C, D). In addition, proteomic analysis of the substantia nigra tissue showed a marked increase in COL1A1 expression in patients with dopaminergic neuron loss [62] (Supplementary Fig. 10E). These findings provide compelling evidence of increased collagen I in the brains of patients with PD and indicate that this change may adversely impact dopaminergic neurons.

To investigate the cellular effects of increased collagen I and the role of synphilin-1 overexpression, we compared cell viability between HEK293 and Synph-293 cells on plates coated with progressively higher concentrations of collagen I on a poly-L-lysine base. HEK293 cells showed gradual reduction in viability as the concentration of coated collagen I increased, with statistical significance at the higher collagen I concentration (Supplementary Fig. 11A). Conversely, Synph-293 cells showed no change in cell viability across varying collagen I concentrations compared with the control, demonstrating resistance to collagen I-induced cytotoxicity (Supplementary Fig. 11B). A comparison of the two cell types revealed a significant difference in cell viability at increased collagen I concentrations (Supplementary Fig. 11C). To further explore these protective effects, we constructed transcriptomic and proteomic networks for Synph-293 cells utilizing IPA. The transcriptomic network predicted reduced ECM binding and cytotoxicity alongside activation of neuroprotection, showing interconnections between these functions via molecular interactions (Supplementary Fig. 11D). The proteomic network revealed similar patterns with the transcriptomic predictions (Supplementary Fig. 11E). Finally, the integrated omics network provided more apparent functional predictions than the single-omics approaches (Supplementary Fig. 11F). These results show that synphilin-1 overexpression may exert a protective effect against toxicity induced by excessive collagen I, which is elevated in PD.

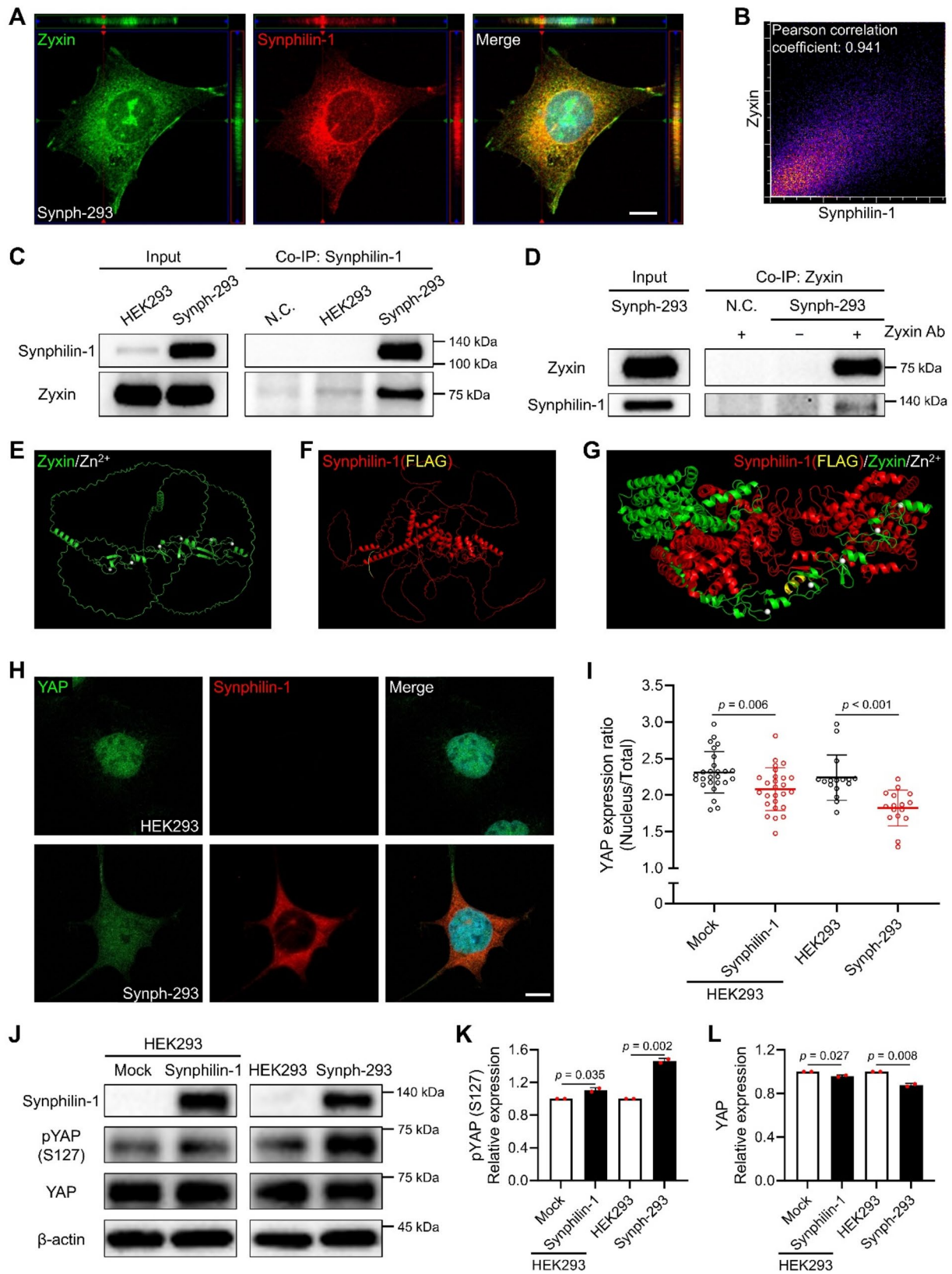


Fig. 5 (See legend on next page.)

(See figure on previous page.)

Fig. 5 Synphilin-1 interacted with zyxin in the cytosol and affected the subcellular location of YAP. **A** Expression patterns of synphilin-1 and zyxin in Synph-293 cells (scale bar: 10 μm). Images represent one z-position of confocal z-stack images. **B** Scatter plot of the pixel intensity of synphilin-1 and zyxin channels of cytosol area. **C, D** Co-immunoprecipitation (Co-IP) assay between synphilin-1 and zyxin. Cells were subjected to cross-linking using 1% formaldehyde before lysis. Cell lysates were immunoprecipitated with synphilin-1 (**C**) and zyxin antibodies (**D**). N.C.: negative control. **E–G** Prediction of single protein and protein-protein structures using AlphaFold 3. Protein structures indicate zyxin with six Zn^{2+} ions (**E**), FLAG-synphilin-1 (**F**), and FLAG-synphilin-1-zyxin with six Zn^{2+} ions (**G**). **H** Subcellular expression pattern of YAP in HEK293 and Synph-293 cells (scale bar: 10 μm). **I** Quantification of nuclear YAP expression intensity ratio in synphilin-1-overexpressing HEK293 cells ($n = 27/27/16/16$). Lines represent the mean \pm SD. Individual value is represented as a hollow circle. **J** Protein expression of Ser127 phosphorylated YAP (pYAP (S127)) and total YAP in synphilin-1-overexpressing HEK293 cells. **K** Relative expression level of pYAP (S127). **L** Relative expression level of total YAP. Data represent the mean \pm SD. Individual value is represented as a red circle. Statistical significance was determined using an independent sample *t*-test with Levene's test

Discussion

In this study, we analyzed the biophysical functions of synphilin-1 in cells using a combined approach involving molecular biology, mechanobiology, and an integrated omics methodology incorporating transcriptomic and proteomic analyses. Our findings demonstrate that synphilin-1 overexpression affected cellular shape and the ability to sense substrate rigidity. Notably, Synph-293-KD cells restored responsiveness to different substrate stiffnesses. Comprehensive analysis of the biophysical mechanism of synphilin-1 overexpression using integrated omics and *in silico* predictions elucidated the molecular mechanisms associated with focal adhesion formation, cell spreading, cellular protrusion retraction, and cell contraction. Furthermore, we identified zyxin as a binding partner of synphilin-1, elucidating its effects on mechanosensing, particularly the synphilin-1 overexpression-induced inhibition of the nuclear localization of YAP.

An elastomeric micropillar array system, specifically PDMS-based submicron pillar arrays, was employed to measure cellular forces. These arrays are recognized for their ability to measure cell-generated forces at the nano-newton level [21, 24, 63]. The system is particularly advantageous for identifying the rigidity sensing ability of cells in the early stages of spreading. This ability is attributed to the cells' recognition of substrate rigidity through actomyosin-based local contractions, which is reflected in the distribution and direction of pillar deflections [27, 51]. The obtained pillar array results show that Synph-293 cells provide insights into the morphological changes observed on flat substrates. On the micropillar arrays, Synph-293 cells exhibit a rounded morphology accompanied by the directed bending of most pillars beneath them toward the center, indicating a lack of local contraction between adjacent pillars. The reduced number of occupied pillars was similar to the observed decrease in cell spreading area on flat substrates, suggesting an alteration in cellular adhesion dynamics. These findings suggest that Synph-293 cells fail to establish robust focal adhesions and lamellipodial protrusions necessary for mechanosensing and spreading. The hindered extension of protrusions toward unexplored pillars likely results in reduced cellular spreading and a retraction toward the

center, reinforcing a passive shrinkage behavior rather than an active substrate exploration. Remarkably, these phenomena were reversed upon synphilin-1 knockdown in Synph-293 cells. Our study revealed that synphilin-1 overexpression induced cellular retraction toward the center, accompanied by diminished local contractions, suggesting a potential role for synphilin-1 in altering cellular morphology and behavior.

Despite the identification of a limited number of locally contracting pillar pairs in the single time point of pillar maps of Synph-293 cell edge, in the pillar high-speed photographs, the presence of step-fitted pillar pairs was exclusively detected in HEK293 and Synph-293-KD cells. This observation suggests a plausible scenario wherein, even if adjacent pillars are connected to form a contractile unit in Synph-293 cells, their functional efficacy appears compromised. Furthermore, our findings directly demonstrated that synphilin-1 overexpression induced the loss of cellular rigidity sensing ability on substrate stiffness, a crucial mechanism in cellular responses to the microenvironment. However, this loss of rigidity sensing proved amenable to effective restoration through synphilin-1 knockdown. These results elucidate the intricate interplay between synphilin-1 expression and cellular responses, highlighting the potential of manipulating synphilin-1 expression to modulate cellular behavior and rigidity sensing in various contexts.

Our findings on PDMS substrates of varying stiffness demonstrated that Synph-293 cells did not respond to substrate stiffness, as there were no changes in cell area or focal adhesions. It suggests that overexpression of synphilin-1 impairs the ability of cells to sense mechanical cues. Supporting this notion, synphilin-1 knockdown restored the responses on diverse substrate stiffness, indicating that synphilin-1 may regulate mechanosensing capacity. In the present study, a detailed relationship between actin and focal adhesions, as well as real-time imaging, was not analyzed. Future studies incorporating co-staining and live-cell imaging in our system will provide a better understanding of synphilin-1's effect on cytoskeletal dynamics and mechanotransduction.

In the context of rapid advancements in high-throughput technologies, omics analyses, encompassing transcriptomics and proteomics, have emerged as

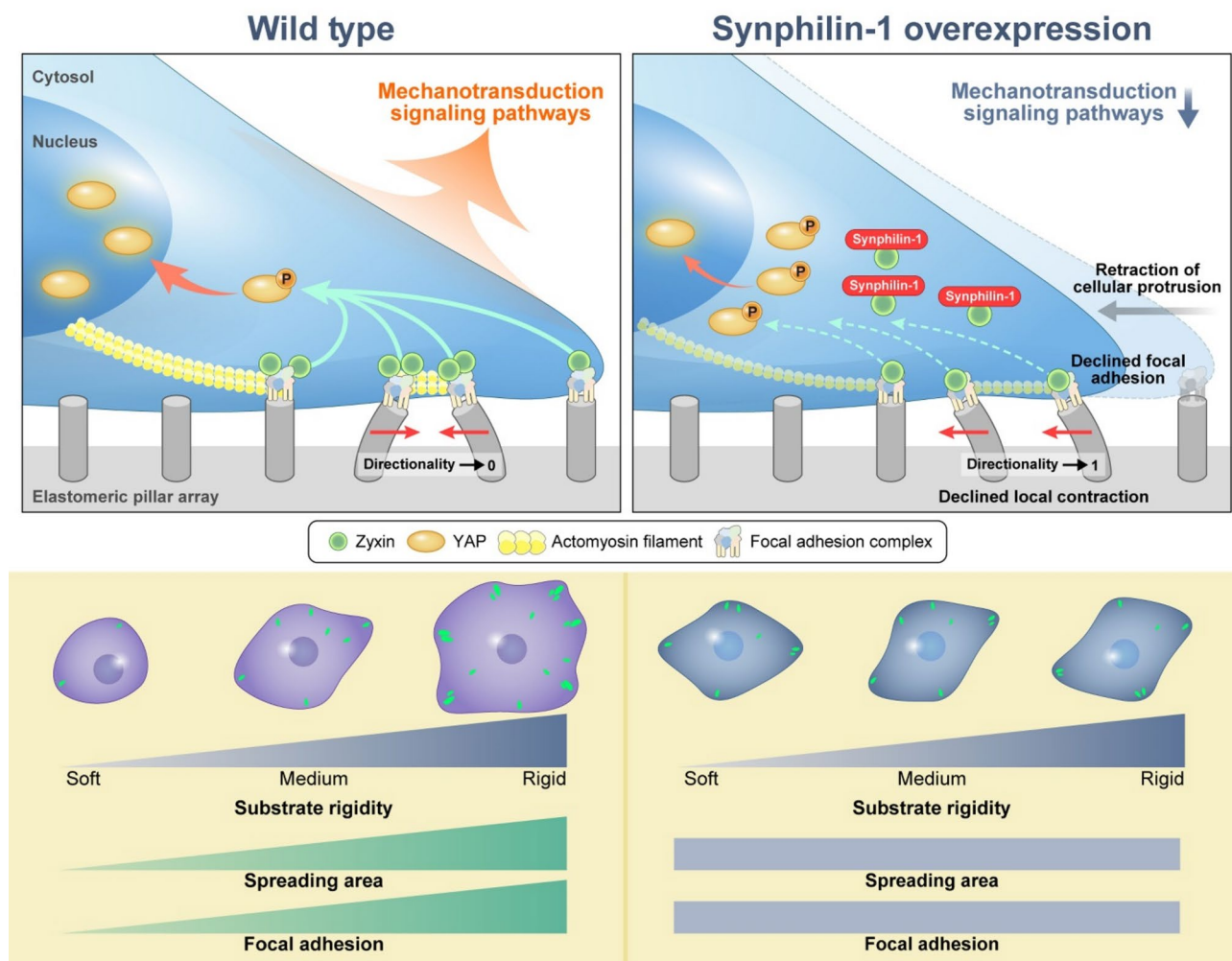


Fig. 6 Synphilin-1 regulated substrate rigidity sensing by interacting with zyxin and affecting YAP localization. Under conditions of synphilin-1 overexpression, the following observations were made. Synphilin-1 interacts with endogenous zyxin in the cytosol. This interaction reduces the transportation of zyxin into complexes containing focal adhesion and causes interference in mechanotransduction signaling, especially signaling through the nuclear translocation of YAP. Therefore, synphilin-1-overexpressing cells on the pillar array are unable to spread to further pillars, and they retract their protrusions. In addition, the synphilin-1-overexpressing cells do not respond to substrates of various stiffness through changes in morphology, including spreading area and focal adhesion. These phenomena can be reversed by synphilin-1 knockdown in cells overexpressing synphilin-1

indispensable tools for unraveling complex biological mechanisms [39]. Each omics analysis offers insights into the molecular expression changes associated with pathology and biological functions, facilitating a closer understanding of the underlying cellular processes [40]. Nevertheless, inherent limitations persist within each singular omics analysis. For example, transcriptomics analysis falls short of elucidating variations in the “end products” pattern, whereas, in proteomics analysis, limitations persist regarding detecting low-abundance proteins [64]. Consequently, multi-omics integration is required to capture the entirety of biological heterogeneity by combining insights from each omics layer [65]. In addition, machine learning-based algorithms can be employed to mitigate biases in omics analyses [65, 66]. In this study, we conducted comprehensive analyses of

the transcriptome and proteome to identify the biophysical functions of synphilin-1, integrating data from both omics layers to counterbalance inherent limitations and maximize the strengths of each single omics analysis. These analyses yielded consistent *in silico* predictions of four biological functions: formation of focal adhesions, cell spreading, retraction of cellular protrusions, and cellular contraction. Omics analysis will be a powerful approach for further elucidating synphilin-1’s functional and physiological roles beyond the mechanobiological perspective. Future studies integrating additional omics layers, such as microRNA, phosphoproteome, and metabolome analyses, with machine learning-based approaches will provide a more comprehensive understanding of synphilin-1’s broader biological significance, including mechanobiological functions.

Zyxin, a focal adhesion protein extensively investigated for its crucial role in cellular mechanotransduction [67], has been implicated in orchestrating cellular responses to substrate rigidity. Notably, fibroblasts subjected to zyxin knockdown exhibited impaired responses to substrate rigidity, manifesting as alterations in the cell area, focal adhesion area, and cell traction stress [35]. Considering the role of zyxin and our results indicating a cytosolic interaction between synphilin-1 and zyxin, it can be inferred that synphilin-1, identified as a novel binding partner of zyxin, may modulate cell morphology and reduce rigidity sensing ability by inhibiting focal adhesions and mechanotransduction signaling. YAP, an evolutionarily conserved mechanotransducer, senses various mechanical signals, such as shear stress, cell shape, and ECM rigidity, translating these inputs into cell-specific transcriptional programs [53]. The cellular localization of YAP was affected by substrate stiffness, with softer substrates promoting cytoplasmic retention and stiffer substrates inducing nuclear translocation [68]. In addition, zyxin has been reported as a positive regulator of YAP signaling, engaging in the mediation of Siah2-Lats2 and CDK8 [54, 55]. Ma et al. demonstrate that zyxin knockdown increases Ser127 phosphorylation of YAP and reduces its nuclear translocation, explaining this mechanism as zyxin forming a ternary complex with Lats2 and Siah2, facilitating Lats2 ubiquitination and degradation, which leads to YAP dephosphorylation and activation [54]. Zhou et al. showed that zyxin knockdown increases Ser127 phosphorylation of YAP, describing the mechanism as zyxin regulating YAP through CDK8 [55]. In this study, we observed a reduction in the nuclear localization of YAP in synphilin-1-overexpressing cells on the glass substrate. However, no difference was observed between HEK293 and Synph-293 cells cultured on PA gel substrates with much lower stiffness than glass substrate. Our findings suggest that synphilin-1 hindered the nuclear translocation of YAP by binding with zyxin, leading to diminished rigidity sensing, particularly on stiff substrates.

While synphilin-1 has been predominantly studied in neuronal tissues, its expression has also been detected in non-neuronal tissues, including the cervix, endometrium, and ovary (The Human Protein Atlas version 24.0, www.proteinatlas.org/ENSG00000064692-SNCA/IP/tissue) [69]. This observation raises the question of whether synphilin-1's role is beyond neuronal systems. Future studies utilizing cells from multiple tissue types would be valuable in determining whether the effects of synphilin-1 are conserved across various cell types, particularly in mechanically dynamic environments.

The effect of synphilin-1 on substrate rigidity sensing may result from its interactions with several proteins, including its binding to zyxin. Li et al. reported

that synphilin-1 enhanced neurite growth in differentiated N1E-115 mouse neuroblastoma cells, whereas synphilin-1 knockdown induced shortened neurite outgrowth [15]. In addition, synphilin-1-overexpressing N1E-115 cells exhibited a reduced cell body area, as observed in HEK293 and SH-SY5Y cells. Synphilin-1 encompasses three domains, namely ankyrin repeats, a coiled-coil domain, and ATP/GTP-binding motifs, which facilitate its binding to various types of cytoplasmic proteins, including α -synuclein, PRKN, SIAH, PINK1, and AMPK [1, 6, 8, 13, 70]. Moreover, synphilin-1 has been reported to bind to phospholipids, including phosphatidic acid, phosphatidylserine, and phosphatidylglycerol, predominantly localized within cellular membranes [14], and to peripheral membrane proteins, such as SH2D3C [12]. Further studies on its interactions with other binding proteins are imperative to understand its biophysical functions fully.

Recent findings highlight the alteration of ECM, particularly collagen I, in PD-affected brains [18, 19]. We identified a significant increase in collagen I expression in the substantia nigra and striatum of patients with PD. This elevation in collagen I likely contributes to increased tissue stiffness, which could adversely affect neuronal survival and function by altering the mechanical properties of the brain microenvironment. A previous study has reported decreased neuronal cell viability with increasing substrate stiffness, as well as reduced neuroprotective effects of hormetic chemicals against 6-hydroxydopamine-induced toxicity in PD models under stiff substrate conditions, thus supporting the findings of the current study [71]. Additionally, Tripathi et al. reported that transcriptomic analysis of dopaminergic neurons from patients with PD exhibiting PINK1/PRKN mutations revealed activation of focal adhesion and ECM receptor pathways [72]. These findings suggest that ECM alterations, particularly increased collagen I deposition, may contribute to the pathophysiology of PD by modulating cellular adhesion and mechanotransduction. Therefore, targeting ECM remodeling or mechanotransduction pathways could represent a novel therapeutic approach for mitigating neuronal vulnerability in PD. We demonstrate that synphilin-1 overexpression confers a protective effect against excessive collagen I-induced cytotoxicity, suggesting a protective mechanism through the regulation of mechanosensing. Further research is warranted to explore the mechanistic underpinnings of ECM-neuron interactions in PD.

Conclusion

Our findings demonstrate a novel biophysical function of synphilin-1 in substrate rigidity sensing through binding with zyxin. In addition, biophysical mechanism analysis using integrated omics enabled a precise and

comprehensive elucidation of the mechanisms underlying focal adhesion formation, cell spreading, retraction of cellular protrusions, and cellular contraction. These mechanobiological and integrated omics-based approaches offer a groundbreaking perspective for elucidating the universal functions of synphilin-1. Moreover, our findings highlight the biophysical role of synphilin-1 in cellular mechanosensing and its potential to mitigate adverse cellular responses to ECM changes associated with PD.

Supplementary Information

The online version contains supplementary material available at <https://doi.org/10.1186/s12951-025-03429-4>.

Supplementary Material 1: Additional file name: Supplementary materials.pdf. Supplementary materials include "Supplementary methods", "Supplementary Figs. 1–11", "Supplementary Tables 1–3", and "Supplementary references". Supplementary Fig. 1: Reduction of spreading area in synphilin-1 overexpressing human embryonic kidney 293 (HEK293) and SH-SY5Y cells. Supplementary Fig. 2: Restoration of local contraction formation and substrate rigidity sensing by synphilin-1 knockdown. Supplementary Fig. 3: Single omics analysis of canonical pathways from Ingenuity Pathway Analysis. Supplementary Fig. 4: Single omics analysis of diseases and biological functions from Ingenuity Pathway Analysis. Supplementary Fig. 5: Single omics analysis and prediction with transcriptomics and proteomics. Supplementary Fig. 6: Integrated omics analysis and prediction with transcriptomics and proteomics. Supplementary Fig. 7: Synphilin-1 co-localization with zyxin in the cytosol. Supplementary Fig. 8: Synphilin-1 interaction with zyxin. Supplementary Fig. 9: Changing of subcellular location of YAP through synphilin-1 overexpression. Supplementary Fig. 10: Elevation of collagen I expression in substantia nigra and striatum of patients with Parkinson's disease. Supplementary Fig. 11: Protective effect of synphilin-1 overexpression on the excessively coated plate with collagen I. Supplementary Table 1: Primer sequences of transcriptomic network-related genes in RT-qPCR. Supplementary Table 2: Profiles of the genes in the Ingenuity Pathway Analysis-based transcriptomic network. Supplementary Table 3: Profiles of the proteins in the Ingenuity Pathway Analysis-based proteomic network

Acknowledgements

The authors thank the Three-Dimensional Immune System Imaging Core Facility at Ajou University for technical assistance and cell imaging.

Author contributions

SGK: Conceptualization; Data curation; Formal analysis; Investigation; Visualization; Methodology; Writing—original draft; Writing—review and editing. JL: Conceptualization; Data curation; Formal analysis; Investigation; Visualization; Writing—original draft. JSH: Formal analysis; Investigation; Writing—original draft. MAUH: Data curation; Formal analysis; Investigation; Visualization. YES: Data curation, Writing—review and editing. JYL: Data curation, Formal analysis, Writing—review and editing. JM: Data curation, Writing—review and editing. MOK: Validation; Resources; Writing—review and editing. GL: Conceptualization; Supervision; Validation; Methodology; Resources; Funding acquisition; Project administration; Writing—review and editing. SP: Conceptualization; Supervision; Validation; Methodology; Resources; Funding acquisition; Project administration; Writing—review and editing. All authors read and approved the final manuscript.

Funding

This research was funded by the National Research Foundation (NRF) grants (RS-2024-00416536, RS-2023-NR076560, RS-2023-00234581, RS-2023-00242443, and RS-2024-00441331) and the Korea Basic Science Institute (KBSI) grant (C523100) through the Ministry of Science and ICT (MSIT) in the Republic of Korea.

Data availability

Transcriptome sequencing and quantification data are available in the GEO database under the accession number: GSE255201. Proteome data are available at MassIVE: MSV000089926.

Declarations

Ethics approval and consent to participate

Not applicable.

Consent for publication

Not applicable.

Competing interests

The authors declare no competing interests.

Author details

¹Department of Molecular Science and Technology, Ajou University, 206 World cup-ro, Suwon 16499, Republic of Korea

²Department of Mechanical Engineering, Sungkyunkwan University, 2066 Seobu-ro, Suwon 16419, Republic of Korea

³Department of Biomedical Sciences, Graduate School, Ajou University School of Medicine, 164 World cup-ro, Suwon 16499, Republic of Korea

⁴Digital Omics Research Center, Korea Basic Science Institute, 162 Yeongudanji-ro, Cheongju 28119, Republic of Korea

⁵Institute of Medical Science, Ajou University School of Medicine, 164 World cup-ro, Suwon 16499, Republic of Korea

⁶Division of Life Science and Applied Life Science (BK21 FOUR), College of Natural Sciences, Gyeongsang National University, Jinju 52828, Republic of Korea

⁷Department of Physiology, Ajou University School of Medicine, 164 World Cup-ro, Suwon 16499, Republic of Korea

⁸Institute of Quantum Biophysics (IQB), Sungkyunkwan University, 2066 Seobu-ro, Suwon 16419, Republic of Korea

⁹Department of MetaBioHealth, Sungkyunkwan University, 2066 Seobu-ro, Suwon 16419, Republic of Korea

Received: 24 February 2025 / Accepted: 1 May 2025

Published online: 14 May 2025

References

- Engelender S, Kaminsky Z, Guo X, Sharp AH, Amaravi RK, Kleiderlein JJ, et al. Synphilin-1 associates with alpha-synuclein and promotes the formation of cytosolic inclusions. *Nat Genet.* 1999;22(1):110–4.
- Tanaka M, Kim YM, Lee G, Junn E, Iwatsubo T, Mouradian MM. Aggregates formed by alpha-synuclein and synphilin-1 are cytoprotective. *J Biol Chem.* 2004;279(6):4625–31.
- Smith WW, Liu Z, Liang Y, Masuda N, Swing DA, Jenkins NA, et al. Synphilin-1 attenuates neuronal degeneration in the A53T alpha-synuclein Transgenic mouse model. *Hum Mol Genet.* 2010;19(11):2087–98.
- Casadei N, Pohler AM, Tomas-Zapico C, Torres-Peraza J, Schwedhelm I, Witz A, et al. Overexpression of synphilin-1 promotes clearance of soluble and misfolded alpha-synuclein without restoring the motor phenotype in aged A30P Transgenic mice. *Hum Mol Genet.* 2014;23(3):767–81.
- Shishido T, Nagano Y, Araki M, Kurashige T, Obayashi H, Nakamura T, et al. Synphilin-1 has neuroprotective effects on MPP(+)-induced Parkinson's disease model cells by inhibiting ROS production and apoptosis. *Neurosci Lett.* 2019;690:145–50.
- Kruger R. The role of synphilin-1 in synaptic function and protein degradation. *Cell Tissue Res.* 2004;318(1):195–9.
- Chung KK, Zhang Y, Lim KL, Tanaka Y, Huang H, Gao J, et al. Parkin ubiquitinates the alpha-synuclein-interacting protein, synphilin-1: implications for Lewy-body formation in Parkinson disease. *Nat Med.* 2001;7(10):1144–50.
- Liani E, Eyal A, Avraham E, Shemer R, Szargel R, Berg D, et al. Ubiquitylation of synphilin-1 and alpha-synuclein by SIAH and its presence in cellular inclusions and lewy bodies imply a role in Parkinson's disease. *Proc Natl Acad Sci U S A.* 2004;101(15):5500–5.

9. Lee G, Tanaka M, Park K, Lee SS, Kim YM, Junn E, et al. Casein kinase II-mediated phosphorylation regulates alpha-synuclein/synphilin-1 interaction and inclusion body formation. *J Biol Chem*. 2004;279(8):6834–9.
10. Tsai YC, Riess O, Soehn AS, Nguyen HP. The guanine nucleotide exchange factor kalirin-7 is a novel synphilin-1 interacting protein and modifies synphilin-1 aggregate transport and formation. *PLoS ONE*. 2012;7(12):e51999.
11. Ryo A, Togo T, Nakai T, Hirai A, Nishi M, Yamaguchi A, et al. Prolyl-isomerase Pin1 accumulates in lewy bodies of Parkinson disease and facilitates formation of alpha-synuclein inclusions. *J Biol Chem*. 2006;281(7):4117–25.
12. Stelzl U, Worm U, Lalowski M, Haenig C, Brembeck FH, Goehler H, et al. A human protein-protein interaction network: a resource for annotating the proteome. *Cell*. 2005;122(6):957–68.
13. Li T, Liu J, Guo G, Ning B, Li X, Zhu G, et al. Synphilin-1 interacts with AMPK and increases AMPK phosphorylation. *Int J Mol Sci*. 2020;21(12):4352.
14. Takahashi T, Yamashita H, Nagano Y, Nakamura T, Kohriyama T, Matsumoto M. Interactions of Synphilin-1 with phospholipids and lipid membranes. *FEBS Lett*. 2006;580(18):4479–84.
15. Li X, Liu Z, Tamashiro K, Shi B, Rudnicki DD, Ross CA, et al. Synphilin-1 exhibits trophic and protective effects against rotenone toxicity. *Neuroscience*. 2010;165(2):455–62.
16. Burnside ER, Bradbury EJ. Manipulating the extracellular matrix and its role in brain and spinal cord plasticity and repair. *Neuropathol Appl Neurobiol*. 2014;40(1):26–59.
17. Downs M, Zaia J, Sethi MK. Mass spectrometry methods for analysis of extracellular matrix components in neurological diseases. *Mass Spectrom Rev*. 2023;42(5):1848–75.
18. Raghunathan R, Hogan JD, Labadorf A, Myers RH, Zaia J. A glycomics and proteomics study of aging and Parkinson's disease in human brain. *Sci Rep*. 2020;10(1):12804.
19. Downs M, Sethi MK, Raghunathan R, Layne MD, Zaia J. Matrisome changes in Parkinson's disease. *Anal Bioanal Chem*. 2022;414(9):3005–15.
20. Ketebo AA, Din SU, Lee G, Park S. Mechanobiological analysis of nanoparticle toxicity. *Nanomaterials (Basel)*. 2023;13(10):1682.
21. Shin TH, Ketebo AA, Lee DY, Lee S, Kang SH, Basith S, et al. Decrease in membrane fluidity and traction force induced by silica-coated magnetic nanoparticles. *J Nanobiotechnol*. 2021;19(1):21.
22. Colin-York H, Shrestha D, Felce JH, Waithe D, Moeendarbary E, Davis SJ, et al. Super-Resolved traction force microscopy (STFM). *Nano Lett*. 2016;16(4):2633–8.
23. Cui Y, Hameed FM, Yang B, Lee K, Pan CQ, Park S, et al. Cyclic stretching of soft substrates induces spreading and growth. *Nat Commun*. 2015;6:6333.
24. Tan JL, Tien J, Pirone DM, Gray DS, Bhadriraju K, Chen CS. Cells lying on a bed of microneedles: an approach to isolate mechanical force. *Proc Natl Acad Sci U S A*. 2003;100(4):1484–9.
25. Wang JH, Thampatty BP. An introductory review of cell mechanobiology. *Biomech Model Mechanobiol*. 2006;5(1):1–16.
26. Jansen KA, Donato DM, Balcioglu HE, Schmidt T, Danen EH, Koenderink GH. A guide to mechanobiology: where biology and physics Meet. *Biochim Biophys Acta*. 2015;1853(1 Pt B):3043–52.
27. Ghassemi S, Meacci G, Liu S, Gondarenko AA, Mathur A, Roca-Cusachs P, et al. Cells test substrate rigidity by local contractions on submicrometer pillars. *Proc Natl Acad Sci U S A*. 2012;109(14):5328–33.
28. Janmey PA, Fletcher DA, Reinhart-King CA. Stiffness sensing by cells. *Physiol Rev*. 2020;100(2):695–724.
29. Ketebo AA, Shin TH, Jun M, Lee G, Park S. Effect of silica-coated magnetic nanoparticles on rigidity sensing of human embryonic kidney cells. *J Nanobiotechnol*. 2020;18(1):170.
30. Gupta M, Doss B, Lim CT, Voituriez R, Ladoux B. Single cell rigidity sensing: A complex relationship between focal adhesion dynamics and large-scale actin cytoskeleton remodeling. *Cell Adh Migr*. 2016;10(5):554–67.
31. Wehrle-Haller B. Structure and function of focal adhesions. *Curr Opin Cell Biol*. 2012;24(1):116–24.
32. Olson HM, Nechiporuk AV. Lamellipodia-like protrusions and focal adhesions contribute to collective cell migration in zebrafish. *Dev Biol*. 2021;469:125–34.
33. Geiger B, Spatz JP, Bershadsky AD. Environmental sensing through focal adhesions. *Nat Rev Mol Cell Biol*. 2009;10(1):21–33.
34. Wang Y, Gilmore TD. Zyxin and paxillin proteins: focal adhesion plaque LIM domain proteins go nuclear. *Biochim Biophys Acta*. 2003;1593(2–3):115–20.
35. Yip AK, Zhang S, Chong LH, Cheruba E, Woon JYX, Chua TX, et al. Zyxin is involved in fibroblast rigidity sensing and durotaxis. *Front Cell Dev Biol*. 2021;9:735298.
36. Smith MA, Blankman E, Deakin NO, Hoffman LM, Jensen CC, Turner CE, et al. LIM domains target actin regulators paxillin and Zyxin to sites of stress fiber strain. *PLoS ONE*. 2013;8(8):e69378.
37. Cattaruzza M, Latratch C, Hecker M. Focal adhesion protein Zyxin is a mechanosensitive modulator of gene expression in vascular smooth muscle cells. *Hypertension*. 2004;43(4):726–30.
38. Yoshigi M, Hoffman LM, Jensen CC, Yost HJ, Beckerle MC. Mechanical force mobilizes Zyxin from focal adhesions to actin filaments and regulates cytoskeletal reinforcement. *J Cell Biol*. 2005;171(2):209–15.
39. Kaur P, Singh A, Chana I. Computational techniques and tools for omics data analysis: state-of-the-art, challenges, and future directions. *Arch Comput Method E*. 2021;28:4595–631.
40. Hasin Y, Seldin M, Lusic A. Multi-omics approaches to disease. *Genome Biol*. 2017;18(1):83.
41. Phukan G, Shin TH, Shim JS, Paik MJ, Lee JK, Choi S, et al. Silica-coated magnetic nanoparticles impair proteasome activity and increase the formation of cytoplasmic inclusion bodies in vitro. *Sci Rep*. 2016;6:29095.
42. Lee G, Junn E, Tanaka M, Kim YM, Mouradian MM. Synphilin-1 degradation by the ubiquitin-proteasome pathway and effects on cell survival. *J Neurochem*. 2002;83(2):346–52.
43. Schindelin J, Arganda-Carreras I, Frise E, Kaynig V, Longair M, Pietzsch T, et al. Fiji: an open-source platform for biological-image analysis. *Nat Methods*. 2012;9(7):676–82.
44. Tan JL, Liu W, Nelson CM, Raghavan S, Chen CS. Simple approach to micropattern cells on common culture substrates by tuning substrate wettability. *Tissue Eng*. 2004;10(5–6):865–72.
45. Schoen I, Hu W, Klotsch E, Vogel V. Probing cellular traction forces by micropillar arrays: contribution of substrate warping to pillar Deflection. *Nano Lett*. 2010;10(5):1823–30.
46. Carvalho PC, Xu T, Han X, Cociorva D, Barbosa VC, Yates JR 3. YADA: a tool for taking the most out of high-resolution spectra. *Bioinformatics*. 2009;25(20):2734–6.
47. Tabb DL, McDonald WH, Yates JR 3. DTASelect and contrast: tools for assembling and comparing protein identifications from shotgun proteomics. *J Proteome Res*. 2002;1(1):21–6.
48. Raso C, Cosentino C, Gaspari M, Malara N, Han X, McClatchy D, et al. Characterization of breast cancer interstitial fluids by TmT labeling, LTQ-Orbitrap Velos mass spectrometry, and pathway analysis. *J Proteome Res*. 2012;11(6):3199–210.
49. Abramson J, Adler J, Dunger J, Evans R, Green T, Pritzel A, et al. Accurate structure prediction of biomolecular interactions with alphafold 3. *Nature*. 2024;630(8016):493–500.
50. UniProt C. UniProt: the universal protein knowledgebase in 2023. *Nucleic Acids Res*. 2023;51(D1):D523–31.
51. Wolfenson H, Meacci G, Liu S, Stachowiak MR, Iskratsch T, Ghassemi S, et al. Tropomyosin controls sarcomere-like contractions for rigidity sensing and suppressing growth on soft matrices. *Nat Cell Biol*. 2016;18(1):33–42.
52. Anderson CA, Kovar DR, Gardel ML, Winkelman JD. LIM domain proteins in cell mechanobiology. *Cytoskeleton (Hoboken)*. 2021;78(6):303–11.
53. Panciera T, Azzolin L, Cordenonsi M, Piccolo S. Mechanobiology of YAP and TAZ in physiology and disease. *Nat Rev Mol Cell Biol*. 2017;18(12):758–70.
54. Ma B, Cheng H, Gao R, Mu C, Chen L, Wu S, et al. Zyxin-Siah2-Lats2 axis mediates Cooperation between Hippo and TGF-beta signalling pathways. *Nat Commun*. 2016;7:11123.
55. Zhou J, Zeng Y, Cui L, Chen X, Stauffer S, Wang Z, et al. Zyxin promotes colon cancer tumorigenesis in a mitotic phosphorylation-dependent manner and through CDK8-mediated YAP activation. *Proc Natl Acad Sci U S A*. 2018;115(29):E6760–9.
56. Basu S, Totty NF, Irwin MS, Sudol M, Downward J. Akt phosphorylates the Yes-associated protein, YAP, to induce interaction with 14-3-3 and Attenuation of p73-mediated apoptosis. *Mol Cell*. 2003;11(1):11–23.
57. Lamar JM, Stern P, Liu H, Schindler JW, Jiang ZG, Hynes RO. The Hippo pathway target, YAP, promotes metastasis through its TEAD-interaction domain. *Proc Natl Acad Sci U S A*. 2012;109(37):E2441–50.
58. Tang VW. Collagen, stiffness, and adhesion: the evolutionary basis of vertebrate mechanobiology. *Mol Biol Cell*. 2020;31(17):1823–34.
59. Simchovitz A, Hanan M, Yayon N, Lee S, Bennett ER, Greenberg DS, et al. A LncRNA survey finds increases in neuroprotective LINC-PINT in Parkinson's disease substantia nigra. *Aging Cell*. 2020;19(3):e13115.
60. Tranchevent LC, Halder R, Glaab E. Systems level analysis of sex-dependent gene expression changes in Parkinson's disease. *NPJ Parkinsons Dis*. 2023;9(1):8.

61. Irmady K, Hale CR, Qadri R, Fak J, Simelane S, Carroll T, et al. Blood transcriptomic signatures associated with molecular changes in the brain and clinical outcomes in Parkinson's disease. *Nat Commun*. 2023;14(1):3956.
62. Petyuk VA, Yu L, Olson HM, Yu F, Clair G, Qian WJ, et al. Proteomic profiling of the substantia nigra to identify determinants of lewy body pathology and dopaminergic neuronal loss. *J Proteome Res*. 2021;20(5):2266–82.
63. du Roure O, Saez A, Buguin A, Austin RH, Chavrier P, Silberzan P, et al. Force mapping in epithelial cell migration. *Proc Natl Acad Sci U S A*. 2005;102(7):2390–5.
64. Karahalil B. Overview of systems biology and omics technologies. *Curr Med Chem*. 2016;23(37):4221–30.
65. Picard M, Scott-Boyer MP, Bodein A, Perin O, Droit A. Integration strategies of multi-omics data for machine learning analysis. *Comput Struct Biotechnol J*. 2021;19:3735–46.
66. Shin TH, Manavalan B, Lee DY, Basith S, Seo C, Paik MJ, et al. Silica-coated magnetic-nanoparticle-induced cytotoxicity is reduced in microglia by glutathione and citrate identified using integrated omics. *Part Fibre Toxicol*. 2021;18(1):42.
67. Martino F, Perestrello AR, Vinarsky V, Pagliari S, Forte G. Cellular mechanotransduction: from tension to function. *Front Physiol*. 2018;9:824.
68. Dupont S, Morsut L, Aragona M, Enzo E, Giulitti S, Cordenonsi M, et al. Role of YAP/TAZ in mechanotransduction. *Nature*. 2011;474(7350):179–83.
69. Karlsson M, Zhang C, Mear L, Zhong W, Digre A, Katona B, et al. A single-cell type transcriptomics map of human tissues. *Sci Adv*. 2021;7(31):eabh2169.
70. Li T, Liu J, Smith WW. Synphilin-1 binds ATP and regulates intracellular energy status. *PLoS ONE*. 2014;9(12):e115233.
71. Zhang C, Tan Y, Feng J, Huang C, Liu B, Fan Z, et al. Exploration of the effects of substrate stiffness on biological responses of neural cells and their mechanisms. *ACS Omega*. 2020;5(48):31115–25.
72. Tripathi U, Rosh I, Ben Ezer R, Nayak R, Hussein Y, Choudhary A, et al. Upregulated ECM genes and increased synaptic activity in Parkinson's human DA neurons with PINK1/PRKN mutations. *NPJ Parkinsons Dis*. 2024;10(1):103.

Publisher's note

Springer Nature remains neutral with regard to jurisdictional claims in published maps and institutional affiliations.